Modelling of the thermal conductivity in polymer nanocomposites and the impact of the interface between filler and matrix

2011 J. Phys. D: Appl. Phys. 44 395401

(http://iopscience.iop.org/0022-3727/44/39/395401)

IOP PUBLISHING JOURNAL OF PHYSICS D: APPLIED PHYSICS

J. Phys. D: Appl. Phys. **44** (2011) 395401 (12pp) doi:10.1088/0022-3727/44/39/395401

Modelling of the thermal conductivity in polymer nanocomposites and the impact of the interface between filler and matrix

R Kochetov[1], A V Korobko[2,3], T Andritsch[1], P H F Morshuis[1], S J Picken[2] and J J Smit[1]

[1] High Voltage Technology and Management Group, Department of Electrical Sustainable Energy, Faculty of Electrical Engineering, Mathematics and Computer Science, Delft University of Technology, Mekelweg 4, 2628 CD, Delft, The Netherlands
[2] NanoStructured Materials, Department of Chemical Engineering, Delft University of Technology, Julianalaan 136, 2628 BL, Delft, The Netherlands
[3] Dutch Polymer Institute, PO Box 902, 5600 AX, Eindhoven, The Netherlands

E-mail: roman.kochetov@gmail.com

Received 9 June 2011, in final form 21 July 2011
Published 9 September 2011
Online at stacks.iop.org/JPhysD/44/395401

Abstract
In this paper the thermal conductivity of epoxy-based composite materials is analysed. Two- and three-phase Lewis–Nielsen models are proposed for fitting the experimental values of the thermal conductivity of epoxy-based polymer composites. Various inorganic nano- and micro-particles were used, namely aluminium oxide, aluminium nitride, magnesium oxide and silicon dioxide with average particle size between 20 nm and 20 μm. It is shown that the filler–matrix interface plays a dominant role in the thermal conduction process of the nanocomposites. The two-phase model was proposed as an initial step for describing systems containing 2 constituents, i.e. an epoxy matrix and an inorganic filler. The three-phase model was introduced to specifically address the properties of the interfacial zone between the host polymer and the surface modified nanoparticles.

(Some figures in this article are in colour only in the electronic version)

1. Introduction

Polymers are promising materials for a broad variety of applications, but low thermal conductivity limits their use. Most polymers have a thermal conductivity between 0.1 and 0.6 $W\,m^{-1}\,K^{-1}$ [1]. In order to improve the thermal conductivity of polymers, inorganic fillers with a higher thermal conductivity than the host, such as aluminium nitride (AlN) [2–8], boron nitride (BN) [3, 4, 6, 9–12], aluminium oxide (Al_2O_3) [4, 10, 13, 14], silicon dioxide (SiO_2) [4, 15, 16], silicon carbide (SiC) [10, 13], silicon nitride (Si_3N_4) [10, 15, 17], carbon nanotubes [18, 19] and nanodiamond [15, 16], are used to create polymer-based composites with improved thermal conduction.

Different scientific groups tried to improve the thermal conductivity of polymers using common and sometimes rather exotic methods and theories. Fukushima *et al* [20] and Miyazaki *et al* [21] have developed a novel material design to improve the thermal conductivity, where isotropic resins align 'themselves', by controlling the higher order structure. The thermal conductivity values of the newly developed resin were up to 5 times higher than those of conventional epoxy resins (ERs), because the mesogens form highly ordered crystal-like structures, which suppress phonon scattering. Ekstrand and co-authors [22] proposed the following: (a) decreasing the number of thermally resistant junctions; (b) forming conducting networks by suitable packing; and (c) minimize filler–matrix interfacial defects to improve the thermal conductivity of the polymer composites. Han *et al* [10] found that an epoxy-filler composite with agglomerates of particles is more efficient in enhancing the thermal conductivity than a nanocomposite (NC) with well dispersed nanoparticles. This is presumably due to formation of percolated pathways or networks.

The thermal conductivity value of composites containing microparticles can be calculated by taking into account the

shape and volume of the incorporated particles, assuming diffusive heat conduction in both phases. This approach cannot be applied to a system with nanoparticles inside. The main purpose of this study is to expand models used to predict the thermal conductivity for solid and liquid electrical insulation materials containing nanoparticles. Various factors have to be taken into consideration for NCs, which can be disregarded when dealing with microscale particles. Interface resistance and phonon scattering become increasingly important in the case of nano-scale particles [23]. The incorporated surface modified nanoparticles reorganize the structure and change the properties of a polymer in the vicinity of the filler. The interfacial layer, which can be defined as a transition layer between a host material and incorporated filler, has different crystallinity, glass transition temperature, crosslink density, permittivity, thermal conductivity, etc [24]. In some cases the physico-chemical micro- and macro-properties of the interfacial layer play a more important role than the properties of the individual components. The properties of the interfacial layer might match neither the properties of the matrix nor the properties of the incorporated filler.

Novel to this work is the description and fitting of the thermal conductivity, taking into account the features inherent to NCs in particular. We propose the three-phase Lewis–Nielsen (LN) model that covers the interface between matrix and embedded filler and Kapitza resistance, caused by different phonon scattering processes.

2. Experimental

2.1. Materials and sample preparation

The polymer matrix used in this study is an ER system based on diepoxide-bisphenol-A with an anhydride-type hardener. The system was chosen because of its low viscosity before curing and good processability. The fillers used were Nanopox®, aluminium oxide, aluminium nitride, magnesium oxide and silicon dioxide. Nanopox® is a commercially available colloidal silicon dioxide sol in an ER matrix. In addition to Al_2O_3, AlN, SiO_2 and MgO nanoparticles, silica and alumina microparticles have also been used for our study. Nano-Al_2O_3 and AlN particles were obtained from Sigma-Aldrich. Nanopox® was supplied by Nanoresins. MgO was provided by Strem Chemicals. Micro-Al_2O_3 and micro-SiO_2 were received from Albemarle and Huntsman, respectively.

The specimens, details and the measured thermal conductivity values are summarized in table 1.

The composites were successfully fabricated using *ex situ* polymerization for silane-treated AlN, Al_2O_3 and MgO nanoparticles.

The as-received nanoparticles were dispersed in ethanol by means of ultrasonication at room temperature to break up any agglomerates. Formic acid was added to adjust the pH value to about 4 for AlN and Al_2O_3 particles and pH 3 for MgO particles to reach the higher zeta-potential [25, 26]. A silane coupling agent (SCA) was added to the solution for functionalization of the particles and the solution underwent further sonication to allow hydrolysis and silanol formation. The modified nanoparticles were dispersed in ER by shear force mixing. Afterwards the solvent was evaporated in a vacuum oven and the composite was consequently mixed with hardener via mechanical stirring prior to degassing. The mixture was cast into pre-heated aluminium molds that had been treated with a release agent. Finally, the composite was cured and postcured. The postcured samples were cleaned with alcohol to remove any residues.

The silica nanoparticles that we used were already synthesized in the form of a colloidal sol in an ER. The NCs containing SiO_2 particles were created by *in situ* polymerization, i.e. simple dilution of concentrated silicon dioxide sol with ER and subsequent mixing with hardener, degassing and curing.

The epoxy composites containing Al_2O_3 or SiO_2 microparticles were fabricated in six steps:

(1) mixing the ER, hardener and filler by conventional mechanical high shear stirring;
(2) degassing;
(3) mixing in an ultrasonic bath;
(4) casting into the molds;
(5) curing;
(6) postcuring.

Various types of epoxy NCs were prepared, filled with nano-Al_2O_3, AlN, MgO and SiO_2 with four different filler concentrations of 0.5%, 2%, 5% and 10% by weight as standard, plus composites containing 15 wt% of Al_2O_3 and SiO_2 and 30 wt% of MgO. In addition, several types of alumina and silica microcomposites were fabricated with a fillgrade of up to 60% by weight. Neat epoxy samples were created as a reference. The samples for thermal conductivity measurements were prepared as plates with dimensions of $110 \times 70 \times 3$ mm.

2.2. Measurement techniques

The surface chemistry of nanoparticles was characterized by a Fourier transform Infrared spectroscopy (FTIR). The spectrum was recorded in the range from 4000 to 450 cm^{-1}.

X-ray diffraction (XRD) was used to identify the crystalline structure and purity of as-received particles. XRD measurements of as-received particles were performed on a Bruker-AXS D8 Advance diffractometer, using a Cu Kα source. The 2θ ranges of the data were taken from 10° to 90° with an increment of 0.02°.

The shape and size distribution as well as particle dispersion was carried out by transmission electron microscopy (TEM) and scanning electron microscopy (SEM).

The thermal conductivity measurements were performed with a Thin Heater Apparatus System (THASYS), produced by Hukseflux Thermal Sensors (figure 1). This system performs a direct measurement which allows the determination of the absolute value of the thermal conductivity. With a combination of a thin heater, two samples of similar thickness and two heat sinks it is possible to generate a homogeneous thermal field with a well defined heat flux through the samples.

Table 1. Specimens investigated and their characteristics.

Specimen	Composite	Fillgrade, volume fraction	Thermal conductivity ($W\,m^{-1}\,K^{-1}$)
Neat ER	Neat epoxy resin	0	0.168
ER-SiO_2-0.5	Epoxy system + 0.5 wt% nano-SiO_2	0.003	0.170
ER-SiO_2-2	Epoxy system + 2 wt% nano-SiO_2	0.011	0.172
ER-SiO_2-5	Epoxy system + 5 wt% nano-SiO_2	0.028	0.177
ER-SiO_2-10	Epoxy system + 10 wt% nano-SiO_2	0.057	0.187
ER-SiO_2-15	Epoxy system + 15 wt% nano-SiO_2	0.088	0.199
ER-Al_2O_3-0.5	Epoxy system + 0.5 wt% nano-Al_2O_3	0.002	0.173
ER-Al_2O_3-2	Epoxy system + 2 wt% nano-Al_2O_3	0.006	0.176
ER-Al_2O_3-5	Epoxy system + 5 wt% nano-Al_2O_3	0.016	0.182
ER-Al_2O_3-10	Epoxy system + 10 wt% nano-Al_2O_3	0.033	0.189
ER-Al_2O_3-15	Epoxy system + 15 wt% nano-Al_2O_3	0.051	0.203
ER-AlN-0.5	Epoxy system + 0.5 wt% nano-AlN	0.002	0.174
ER-AlN-2	Epoxy system + 2 wt% nano-AlN	0.007	0.179
ER-AlN-5	Epoxy system + 5 wt% nano-AlN	0.019	0.188
ER-AlN-10	Epoxy system + 10 wt% nano-AlN	0.039	0.205
ER-MgO-0.5	Epoxy system + 0.5 wt% nano-MgO	0.002	0.171
ER-MgO-2	Epoxy system + 2 wt% nano-MgO	0.007	0.175
ER-MgO-5	Epoxy system + 5 wt% nano-MgO	0.017	0.184
ER-MgO-10	Epoxy system + 10 wt% nano-MgO	0.036	0.200
ER-MgO-30	Epoxy system + 30 wt% nano-MgO	0.126	0.262
ER-Al_2O_3-5 (m)	Epoxy system + 5 wt% micro-Al_2O_3	0.016	0.182
ER-Al_2O_3-10 (m)	Epoxy system + 10 wt% micro-Al_2O_3	0.033	0.197
ER-Al_2O_3-20	Epoxy system + 20 wt% micro-Al_2O_3	0.070	0.233
ER-Al_2O_3-30	Epoxy system + 30 wt% micro-Al_2O_3	0.115	0.283
ER-Al_2O_3-40	Epoxy system + 40 wt% micro-Al_2O_3	0.168	0.361
ER-Al_2O_3-50	Epoxy system + 50 wt% micro-Al_2O_3	0.232	0.487
ER-Al_2O_3-60	Epoxy system + 60 wt% micro-Al_2O_3	0.312	0.675
ER-SiO_2-5 (m)	Epoxy system + 5 wt% micro-SiO_2	0.028	0.183
ER-SiO_2-10 (m)	Epoxy system + 10 wt% micro-SiO_2	0.057	0.201
ER-SiO_2-15 (m)	Epoxy system + 15 wt% micro-SiO_2	0.088	0.221
ER-SiO_2-20	Epoxy system + 20 wt% micro-SiO_2	0.120	0.251
ER-SiO_2-40	Epoxy system + 40 wt% micro-SiO_2	0.267	0.408
ER-SiO_2-60	Epoxy system + 60 wt% micro-SiO_2	0.450	0.734

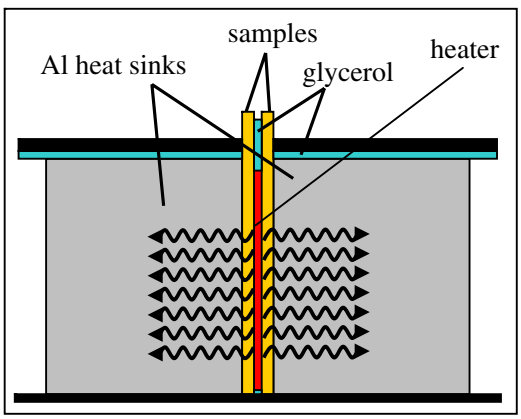

Figure 1. Schematic representation of the working principle of the THASYS.

A straightforward calculation of the thermal conductivity was made using the following equation:

$$\lambda = \varphi \cdot H_{\text{eff}}/\Delta T, \tag{1}$$

where λ is the thermal conductivity, φ is the heat flux derived from the heater power, H_{eff} is the effective sample thickness and ΔT is the temperature difference across the samples.

The thermal conductivity data represents the average value for the thermal conductivity of both samples. The measurements are performed in a climate chamber at 18 °C to avoid any influence due to changes of the ambient temperature during measurement. The accuracy of the measurements is 6%. Each data point corresponds to an average value of 4 measurements. The scatter of the results was negligible, i.e. 0.001 $W\,m^{-1}\,K^{-1}$ maximum.

3. Thermal conductivity models

3.1. Two-phase models

Different theoretical and empirical approaches are available to predict and fit the thermal conductivity of two-phase systems, including the classical works of Nielsen [27, 28], Bruggeman [29], Maxwell [30] and Fricke [31]. They developed models for the effective thermal conductivity of a composite with spherical or spheroidal particles.

The simplest three are the rule of mixture (parallel model, arithmetic mean):

$$\lambda_c = \phi \cdot \lambda_f + (1-\phi)\lambda_m, \tag{2}$$

the inverse rule of mixture (series model, harmonic mean):

$$\frac{1}{\lambda_c} = \frac{\phi}{\lambda_f} + \frac{1-\phi}{\lambda_m}, \tag{3}$$

and the geometric mean, giving the thermal conductivity as

$$\lambda_c = \lambda_f^{\phi} \cdot \lambda_m^{(1-\phi)}, \tag{4}$$

here λ_c, λ_f, λ_m are the thermal conductivities of composite, filler material and polymer matrix, respectively, and ϕ is the filler volume fraction.

The parallel model typically overestimates the thermal conductivity of a composite (upper limit), while the series model tends to predict the lower limit of the thermal conductivity of a two component system. The upper or lower boundaries of the thermal conductivity are given when filler particles are arranged in either parallel or series with respect to the heat flow. Since the particles have a random distribution and are not aligned in direction of the heat flow in the polymer, the parallel and series model do not give us a good prediction of the thermal conductivity of the composites. Maxwell's formula, Lewis and Nielsen theory and the Agari and Uno model are also used for the calculation of the thermal conductivity of composites [32].

To start with analysis, let us consider the LN model adopted from the Halpin–Tsai (HT) mechanical model [33]. The semi-empirical LN model is based on the particle size, geometry, and the manner of particle packing in the matrix. Using the following formulae one can do the basic estimations regarding the thermal conductivity. According to LN theory for composites

$$\lambda_c = \lambda_m \frac{1 + \xi\eta\phi_f}{1 - \Phi\eta\phi_f}, \tag{5}$$

where $\eta = (\lambda_f - \lambda_m)/(\lambda_f + \xi\lambda_m)$ and $\Phi = 1 + ((1 - \phi_M)/\phi_M^2)\phi_f$.

The constant ξ depends on the shape, orientation and aspect ratio of the dispersed particles. The factor ϕ_M represents the maximum packing fraction of the dispersed particles, which is sensitive to the filler shape. The relation $\eta = (\lambda_f - \lambda_m)/(\lambda_f + \xi\lambda_m)$ is coupling the conductivities of the components and the geometry of the filler. The factor Φ was introduced to take the maximum possible concentration of particles into account. For randomly packed spherical particles, $\xi = 1.5$ and $\phi_M = 0.637$.

At the limits of $\xi \to 0$ (for particles with low aspect ratio) and $\xi \to \infty$ (for particles with high aspect ratio), the LN equation reduces to the series $\lambda_c^{-1} = \lambda_f^{-1}\phi_f\Phi + \lambda_m^{-1}(1 - \phi_f\Phi)$ or parallel $\lambda_c = \lambda_f\phi_f + \lambda_m(1-\phi_f)$ thermal conductivity models. Limits show that the maximum packing conditions (Φ) only affect the series model.

The HT expression for the thermal conductivity and canonical form of the parallel and series models can be restored by setting $\Phi = 1$. It is seen and accepted that not the size but the geometry of the filler is responsible for the thermal conductivity of composite materials. Experimental evidence and theoretical modelling support the idea that the most effective heat transport in composites or nanofluids is achieved with rods and platelets, whereas composites with spheres conduct less efficiently [34–37]. Furthermore, a clustering of particles of any shape can significantly increase the thermal conductivity of composites [38].

Similarly Maxwell's formula for a two-phase mixture, consisting of randomly distributed, noninteracting, homogeneous spheres in a homogeneous medium can be used:

$$\lambda_c = \frac{\lambda_f + 2\lambda_m + 2\phi(\lambda_f - \lambda_m)}{\lambda_f + 2\lambda_m - \phi(\lambda_f - \lambda_m)}. \tag{6}$$

This model predicts the thermal conductivity of composites for filler concentrations low enough that filler particles do not touch each other. This expression can also be obtained from the LN model by fixing the value of the shape factor to 2 and the maximum packing factor $\Phi = 1$. Not surprisingly, the value of the shape factor for the Maxwell model is the closest to the one of spherical particles, and therefore is the best for predicting the thermal conductivity of NCs filled with isolated spherical objects.

To extend the overview to the thermal conductivity modelling, we can point to a semi-empirical model proposed by Agari and Uno [39]:

$$\log\lambda_c = \phi \cdot C_2 \cdot \log\lambda_f + (1 - \phi) \cdot \log(C_1 \cdot \lambda_m), \tag{7}$$

where C_1 and C_2 are adjustable constants, which should be determined from experimental data. C_1 indicates the effect of the filler on the secondary structure of the polymer matrix, e.g. crystallinity. The C_2 parameter indicates how easily the particles can form conductive paths inside the polymer [40]. The Agari and Uno model does not really predict thermal conductivity, but basically is a fit function.

3.2. Three-phase LN model

For NCs, a thermal expansion mismatch and poor chemical adhesion of the polymer to the particle surface may lead to inefficient transport of phonons through the interface. This is the so-called interfacial thermal resistance (Kapitza's resistance of an interphase boundary). It provides a temperature discontinuity at the particle–polymer interface, which vanishes when the particle size is above about 100 nm.

The effect of thermal resistance was implemented into the two-phase LN model by introducing the Kapitza's resistance R_K to be in series with the particle resistance, d/λ_f, where d is the particle size. The equivalent resistance then is $d/\lambda_F' = d/\lambda_f + R_K$, and the effective thermal conductivity of a particle including interfacial resistance can be written as [41]

$$\lambda_F' = \frac{\lambda_f}{1 + \frac{R_K\lambda_f}{d}}. \tag{8}$$

In case of very small particles the term R_K/d converges to infinity, $R_K/d \to \infty$, The filler is not involved in the thermal conductivity and the effective thermal conduction of particle is zero, $\lambda_F' = 0$. For large particles the interfacial resistance is not important, since $R_K/d \to 0$.

Let us consider another important point of NCs—surface modification of the filler. The surface treatment increases the contact between particles and the polymer matrix, decreasing the interfacial thermal resistance. Therefore, the transport of the energy through the filler–polymer interface increases. In addition, the modified polymer forms a structure around

the particle, which may differ from the structure of the polymer matrix in the bulk [42, 43]. This layer has a different thermal conductivity compared with the bulk material, but most importantly, the thickness of this layer should not strongly depend on the size of a particle. Thus, the volume of layer is negligibly small for large particles with respect to the particle volume, and will be significant for nanosized particles. The three-phase model is well accepted in the nanofluid community. In nanofluid three-phase models the particles are also subjected to Brownian motion and clustering, in addition to the layering of the liquid at the particle–liquid interface (see recent reviews and references therein [44, 45]). For polymer composites, the high viscosity of the matrix before curing significantly slows down the Brownian motion. The effect of the interfacial shell on the nanofluid conductivity has been analysed by introducing 'complex nanoparticle', the effective particle with thermal properties of the nanoparticle itself and the surrounding interfacial layer [46]. This modification has been done to the original Maxwell [47] and Bruggeman [48] models, although other approaches are reported as well [44], to account for the shape of the particles, clustering and the interfacial thermal resistance [49].

In our case a composite material can be represented by composite particles embedded into the polymer matrix. A 'composite particle' (CP) consists of a particle and the polymer close to the particle surface, which is organized by the surface modification. A CP has a volume $v = v_f + v_l$, where v_f is the volume of a particle and v_l is the volume of layer surrounding this particle. Inspired by the thermal resistance model, the thermal conductivity can be modelled after the series model for the filler-layer CP

$$\frac{1}{\lambda'_F} = \frac{v_f}{\lambda_f(v_f + v_l)} + \frac{v_l}{\lambda_l(v_f + v_l)},$$

where $v_f/(v_f + v_l)$ is the volume fraction of the filler in the CP. For large particles, i.e. $v_f \gg v_l$, we come to $\lambda'_F = \lambda_f$.

The second aspect important in modelling of the interfacial layer in this case is the volume fraction of the CPs, which also includes the volume fraction of the polymer layer. Therefore, we can write $\phi_m + \phi_f + \phi_l = 1$, where the first contribution is from the matrix, the second and the third are from the filler and the interfacial layer, respectively. For spherical particles of radius r, the volume of the interfacial layer is proportional to the volume of the particle. Therefore, the volume of CPs will be written as $\phi_{cp} \equiv \phi_f + \phi_l = \phi_f\delta$, where $\delta = (1 + l/r)^3$ with l being the thickness of the interfacial layer. In this case, the LN expression for two-phase model (equation (5)) together with equation (8) will be modified in three-phase LN model, where $\phi_f\delta$ appears instead of ϕ_f, and $\lambda_f \mapsto \lambda'_F$.

Underlying the aforementioned, we should stress the fact that at small concentrations the condition $\lambda_m = \lim_{\phi_f \to 0}\lambda_c$ must remain valid, if no aggregates or networks of particles are formed.

To determine the volume fraction of the filler for a given weight fraction, the following relation was used:

$$\phi = \frac{W}{W + (1 - W)\frac{\rho_f}{\rho_m}}, \qquad (9)$$

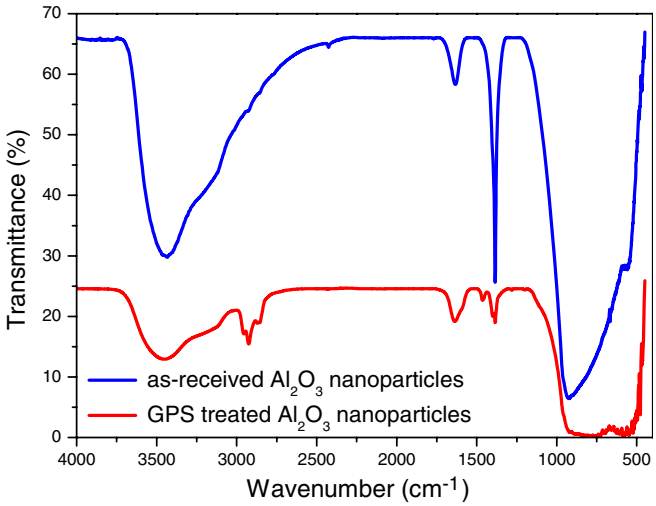

Figure 2. FTIR spectra of untreated and GPS treated nanoalumina particles.

where ϕ is the volume fraction of the filler additives, W is the weight fraction, ρ_f and ρ_m are the densities of the filler and matrix, respectively [6].

4. Results and discussion

4.1. Surface modification of nanoparticles

A SCA was used to improve the interface and adhesion between the inorganic filler and polymer binder. The particle surface modification was performed with an epoxyde-functionalized SCA, namely γ-glycidoxypropyltrimethoxysilane (GPS). AlN, Al_2O_3 and MgO particles have a thin layer of hydroxide on their surface at room temperature [50]. The hydroxyl groups on the surface of the nanoparticles can accelerate the hydrolysis reaction and silane reacts with these hydroxyl groups [51, 52]. The effect of the coupling agent is an alteration of the adhesion between filler and polymer matrix in the composite, which in turn can change the composite properties [53–55].

An example of the FTIR spectra of as-received and GPS treated nanoalumina particles are shown in figure 2.

It can be noticed that the spectrum of as-received (nonmodified) particles has a broad peak at around 3442 cm^{-1} due to hydroxyl groups on the surface of the nanoparticles that are bound either to absorbed water molecules or to each other, via hydrogen bonding. The small peak at 1634 cm^{-1} indicates the deformation of OH groups or water molecules [56]. After surface treatment the peak corresponding to OH groups was reduced. This indicates a reaction of GPS with the functional OH groups on the surface of the Al_2O_3 particle. The FTIR spectrum of functionalized particles shows two peaks at 2929 and 2858 cm^{-1}, which are corresponding to asymmetrical and symmetrical stretching of CH_3 and CH_2. The GPS contains both groups in its chemical structure. The peak of nonmodified particles at around 924 cm^{-1} corresponds to stretching vibrations of Al–O bonds. Summarizing, FTIR analysis indicates a broad OH peak in the region 3000–3700 cm^{-1} for the nonmodified particles and shows that the SCA can react with these hydroxy functional groups,

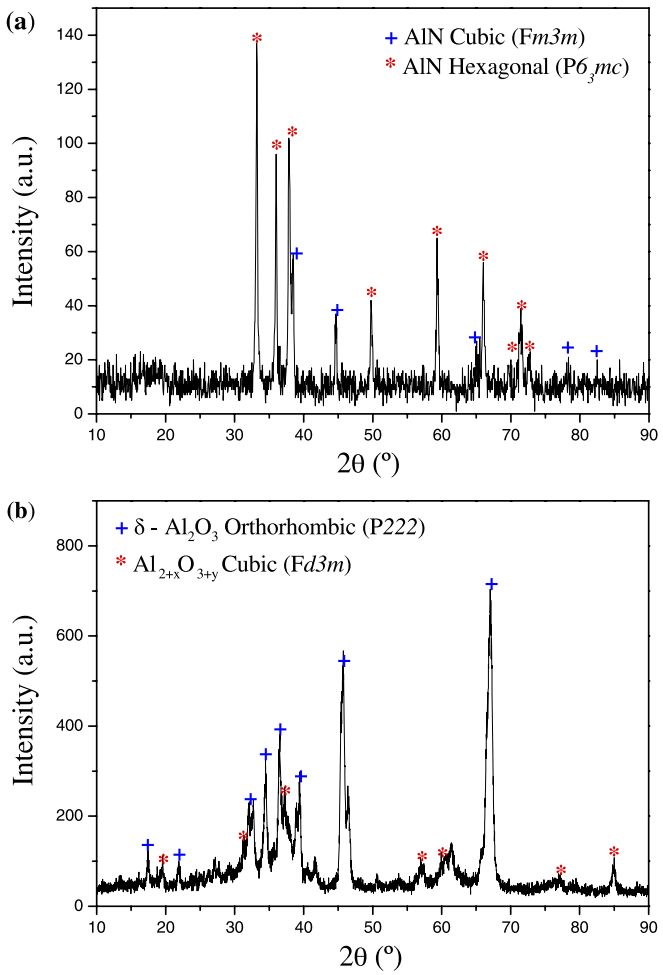

Figure 3. XRD spectra of AlN (*a*) and Al_2O_3 (*b*) nanoparticles.

subsequently allowing chemical and physical bonding between the alumina nanoparticles and the epoxy polymer matrix. FTIR analysis therefore confirmed that the GPS was successfully grafted on the alumina nanoparticles surface.

4.2. Morphological characterization

XRD analysis shows that all particles have a crystalline structure. See figure 3(*a*) as an example, where AlN particles are present in a cubic and hexagonal crystalline structure. Al_2O_3 particles have orthorhombic and cubic crystalline structure as shown in figure 3(*b*).

TEM observation confirms that AlN nanoparticles are crystalline and have different shapes: cubic, spherical and hexagonal. The particles ranged in size from 20 to 500 nm, with 70% being smaller than 100 nm with an average around 60 nm. Al_2O_3 particles have spherical particles with a size distribution between 10 and 200 nm and an average diameter of approximately 30 nm. The TEM images of as-received AlN and Al_2O_3 nanoparticles are presented in figure 4. MgO and SiO_2 particles show a narrow size distribution and an average diameter of 22 nm and 20 nm, respectively. The MgO nanoparticles have crystalline structure and present spherical, ellipsoidal, egg and truncated cubic shapes (figure 5), while SiO_2 are only present in a spherical form. The silica and alumina microparticles have a polycrystalline structure and an irregular shape, their size distribution is broad. The micro-aluminium oxide (Al_2O_3) and silicon dioxide (SiO_2) particles have an average particle size of 4 μm and 20 μm, respectively. The average particle size was determined by averaging over 150 particles of each type.

Figure 6 shows TEM images of ER-Al_2O_3-2 and ER-SiO_2-2 NCs. The pictures suggest a homogeneous dispersion of the alumina and silica fillers in the polymer matrix.

The fabricated composites are classified into three types:

- NCs—the dispersion is good and the size of agglomerations (if they are observed) is not more than 100 nm;
- mesocomposites—the clusters of particles are larger than 100 nm but smaller than 500 nm; and
- microcomposites—the clusters of particles are larger than 500 nm.

Samples of ER with 0.5 wt%, 5 wt% and 10 wt% of Al_2O_3 and SiO_2 were investigated as well. The quality of the dispersion allows one to conclude that the majority of samples with alumina and silica can be labelled as NCs.

Nanoparticles have a strong tendency to agglomerate and form larger particle aggregates [57, 58]. Despite the preventive measures to avoid agglomeration, some composites had aggregates of particles of up to 400 nm for AlN, and

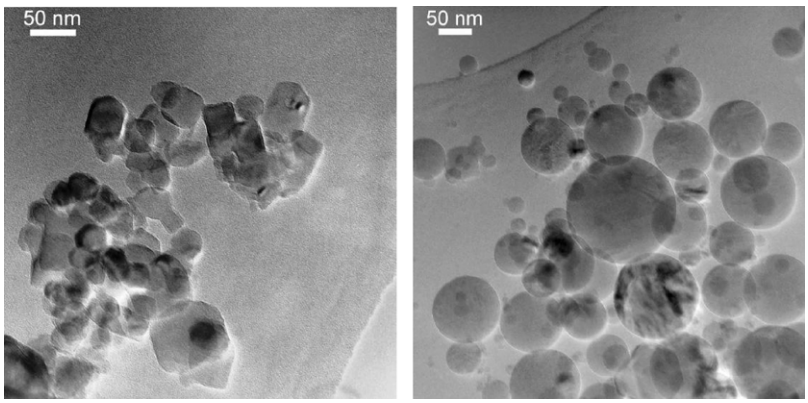

Figure 4. TEM micrographs of as-received AlN (left) and Al_2O_3 particles (right).

up to 200 nm for Al_2O_3 nanofiller material. However, these clusters are well dispersed in the polymer volume. ER-AlN-5, ER-AlN-10, ER-Al_2O_3-10, ER-MgO-10 systems might be considered mesocomposites; while ER-Al_2O_3-0.5, ER-Al_2O_3-2, ER-Al_2O_3-5, ER-AlN-0.5, ER-AlN-2, ER-MgO-0.5, ER-MgO-2, ER-MgO-5 are all NCs.

Ultrathin slices of the sample for TEM analysis were obtained using a diamond knife on an ultramicrotome.

The dispersion state of micro-Al_2O_3 and SiO_2 was determined by SEM. A representative example of the distribution of microparticles inside ER is given in figure 7. The microparticles do not aggregate up to 60 wt%.

4.3. Analysis and modelling

Adding the fillers with a thermal conductivity higher than the epoxy improves the heat transfer of epoxy-based composites. The thermal conductivity of the ER-Al_2O_3 and ER-SiO_2 microcomposites as a function of the filler concentration is shown in figure 8. With an increase in the filler content, the thermal conductivity gradually increases, as anticipated. Incorporation of Al_2O_3 particles in an epoxy matrix resulted in a steady increase of the thermal conductivity by about a factor of 3 at the volume fraction of 0.312. However, to reach the same effect with SiO_2 particles (factor of 3.4), a volume fraction of about 0.45 is required. By adding the same weight amount of microparticles (60 wt%), we get different volume fraction because of the different densities of silica and alumina. For the same volume fraction of microparticles, an ER-Al_2O_3 compound will result in a higher thermal conductivity value than an ER-SiO_2 system.

The size of the particles and their shape play an important role in the heat transfer between polymer matrix and the incorporated filler. Fillers with a higher thermal conductivity than ER improve the heat transfer of composites, considering that the epoxy is a thermal barrier for heat propagation, while the filler material transmits the heat much faster. The thermal conductivity of the mineral alumina, e.g., is more than 10 times higher than that of epoxy. But the resulting values are much lower than the values of bulk crystalline silica or alumina would suggest, because the thermal conductivity of powders is significantly lower than their crystalline bulk counterparts [59]. Since the thermal conductivity of bulk Al_2O_3 is higher than SiO_2, microparticles of alumina will transfer heat more effectively in the compound at the same volume fraction of filler inside the polymer.

The thermal conductivity of NCs might have a completely different mechanism in contrast to microcomposites. In the case of microcomposites the heat is transported by microparticles much faster than in ER. Phonons, which are responsible for heat conduction in dielectric materials, are scattered at the interface between dissimilar materials. The heat dissipates on the surface of nanoparticles to a higher degree than on the surface of microparticles. In the case of NC systems with surface modified filler, the heat transport is controlled by the interface provided by a coupling agent that connects inorganic particles on one side and the polymer host on the other side. The surface functionalized nanoparticles can lead to restructuring of the polymer host and alignment of polymer chains perpendicular to the nanoparticle surface [42].

Figure 9 shows the thermal conductivity behaviour of NCs filled with different types of particles. The thermal conductivity of neat ER might vary in the range $0.170 \pm 0.02\,W\,m^{-1}\,K^{-1}$. These variations are attributed to the minor differences in the epoxy and hardener ratio and time and temperature of polymerization of individual samples [60]. With a filler loading of 10 wt% for AlN, the thermal conductivity of the composite reached $0.205\,W\,m^{-1}\,K^{-1}$.

The higher heat conduction of AlN filled samples can be due to a combination of several factors. First of all, the

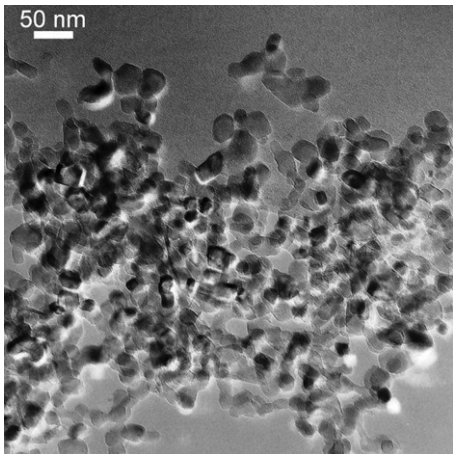

Figure 5. TEM pictures of as-received MgO nanoparticles.

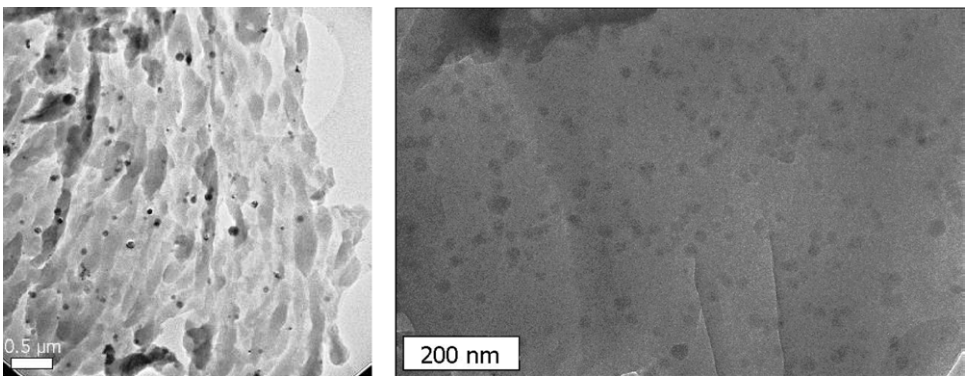

Figure 6. TEM pictures of ER with 2 wt% of Al_2O_3 (left) and 2 wt% of SiO_2 (right).

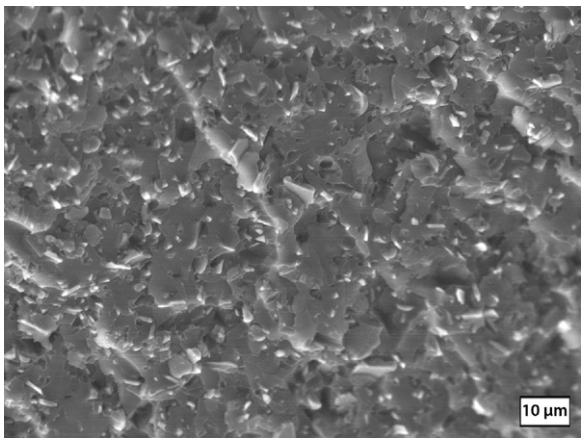

Figure 7. SEM picture of ER-Al_2O_3-40.

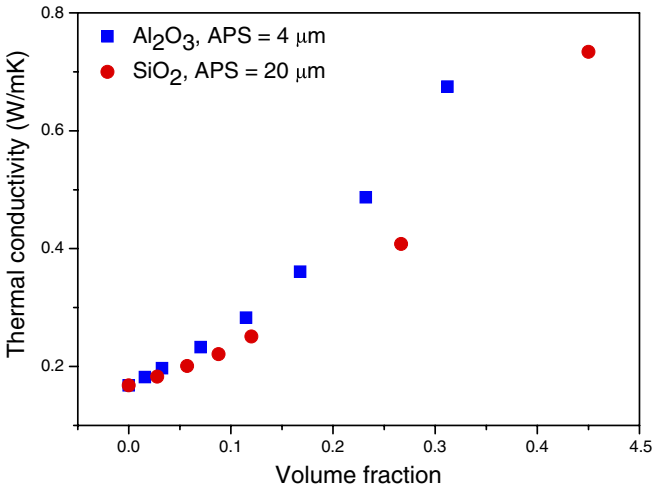

Figure 8. Thermal conductivity of investigated microcomposites as a function of filler volume fraction.

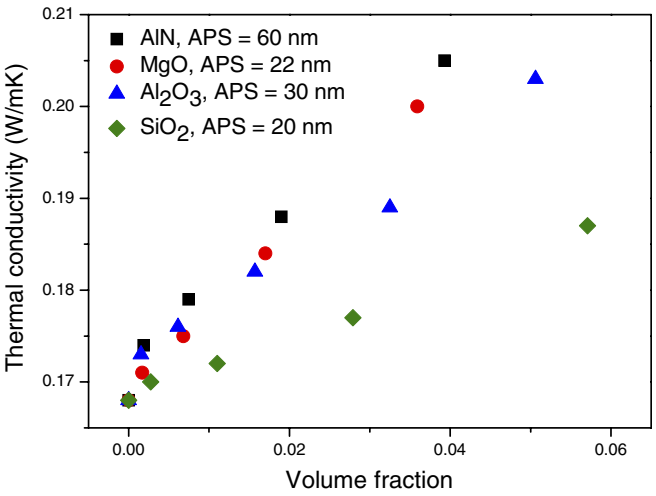

Figure 9. Thermal conductivity of composites with different type of filler versus volume fraction.

structure of AlN suits the criteria for high-thermal conductive materials [59] better than alumina, silica or MgO. Secondly, the higher values of AlN-mesocomposites can be attributed to a large amount of agglomerates, which promote fast heat

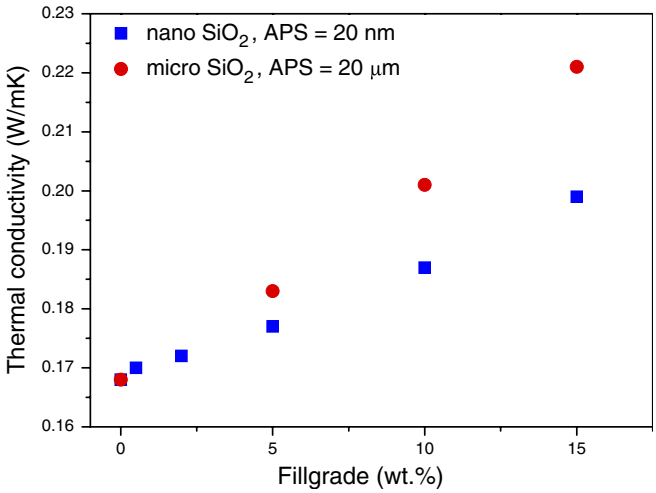

Figure 10. Thermal conductivity of composite with nano- and microparticles of SiO_2 versus fillgrade.

conduction [34]. In addition, the small size of Al_2O_3, SiO_2 and MgO particles leads to large interfacial areas and interfacial thermal resistance, which cause higher levels of phonon scattering. Furthermore, the shape of alumina and silica particles is spherical, while that of AlN is hexagonal and cubic. Particles with an aspect ratio > 1 exhibit better heat conduction in one direction, compared with spheres (aspect ratio $= 1$), with the same volume fraction. The lowest value of thermal conductivity for ER-SiO_2 NCs may be due to the small size of the particles with a nonmodified surface. Due to the lack of modification, the contact between filler and matrix is not fully achieved, thus decreasing the thermal transport across the interface. During the composite preparation, the surface modification of particles not only improves the filler's contact with the matrix, but also changes the structure of the polymer in the proximity of a particle.

The effect of size on the thermal conductivity is revealed in figure 10, where SiO_2 particles are used as filler. The epoxy-based composites filled with SiO_2 microparticles have higher thermal conductivity values, compared with those filled with nanosized particles. This effect is attributed to the phonon scattering on the much larger surface areas of the nanoparticles.

All the data have been fitted to the two-phase and three-phase LN model discussed above. The three-phase model includes the matrix, the filler and the interfacial layer between the matrix and the filler as phases with distinct thermal conductivity and volume. The thermal conductivity and the volume of the interfacial phase are unknown, but we made an attempt to predict those values. It is important to note that the value of the thermal conductivity for the filler is also unknown. The three unknown quantities (λ_f, λ_l and v_l) are estimated by fitting experimental data to the model. To resolve this uncertainty, additional measurements of the interfacial layer may be helpful. There is indirect evidence of the presence of the interfacial polymer layer. For example, the investigation of the complex permittivity of systems containing a low amount of surface modified nanoparticles [42, 61, 62] shows a unique behaviour, which cannot be explained by classical rules of mixture. The epoxy-based composites containing Al_2O_3

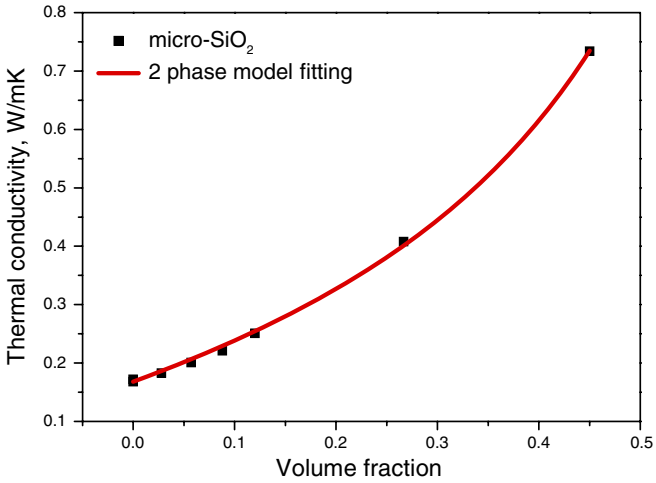

Figure 11. Thermal conductivity of ER-SiO_2 microcomposite as a function of the filler loading (squares) fitted with the 2-phase LN model (solid line).

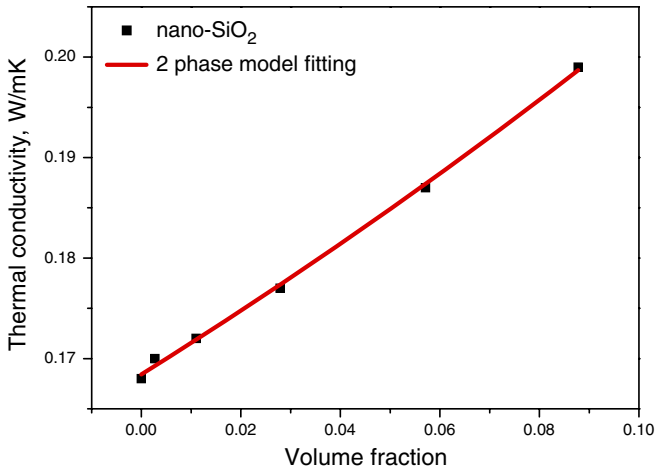

Figure 12. Thermal conductivity of ER-SiO_2 NC as a function of the filler loading (squares) fitted with the 2-phase LN model (solid line).

and MgO nanoparticles showed a reduction in the relative permittivity compared with neat ER. The interface polymer layer leads to immobilization of the epoxy chains around the particles, since the host polymer and filler have strong interaction bonding. A small amount of surface functionalized nanoparticles restructure a large overall volume in the vicinity of the particles. The changes caused by reorganization of polymer material are attributed to the specific properties of the interfacial layer created by the surface modified nanoparticles.

As a representative example, figures 11 and 12 display the fitting of the two-phase LN model (equation (5)) to the experimental data of SiO_2 micro- and nanoparticle composites. The best fitting was achieved with values for the parameters as presented in table 2. The average shape factor of the silica microparticles from fitting appears to be 4.9, which indicates the formation of aggregates. This value is obtained from fitting the model over all fractions of particles, and therefore may reflect a value averaged over all concentrations. In contrast, the data for the NCs are well described by the model with the shape factor value equal to 1.5, which corresponds to homogeneously dispersed spheres. Therefore, we may conclude that nanoparticles do not form clusters, which was also found from TEM observations (figure 6). The maximum packing fraction ϕ_M of the dispersed particles was taken according to the literature with a value of 0.637 [63] for SiO_2 nanoparticles. This results in a value of 0.89 for the term $(1-\phi_M)/\phi_M^2$, as shown in table 2. Only these particles are well dispersed for all concentrations, they are spherical and have a narrow size distribution. The value of ϕ_M for other particles was chosen smaller, since they have a wider size distribution or a shape different than a sphere, which reflects in the values found in table 2.

For the nonspherical particles we assumed agglomeration in the form of a rod-like shape. The thermal conductivity of the composite was calculated by averaging over the isotropic agglomerate orientations, as it was done in literature for the Young modulus estimated by the HT model [64]. The resulting expression for the thermal conductivity becomes $\lambda_c = 5/8 \cdot \lambda_c^{HT}(\xi_1) + 3/8 \cdot \lambda_c^{HT}(\xi_2)$, where λ_c^{HT} is taken from the HT model. The shape factor (ξ_1) equals 2 for the first term and is variable for the second term (ξ_2). The result of the fitting is shown in table 2 for an ER-Al_2O_3 microcomposite (in brackets). There is no significant change in the shape factor, which indicates small aggregates of a few particles.

The results of fitting three-phase (equation (5) and equation (8)) LN models to the experimental data for AlN and MgO are displayed in figures 13 and 14. The three-phase LN model predicts the values for thermal conductivity and the volume of the interfacial phase as shown in table 3. For the three-phase model, the effective volume of the CP is $v_f + v_l$, and the effective value of the filler fraction becomes $\phi_f + \phi_l$. Estimations show that the volume of the interfacial layer takes about 10–40% of the nanoparticle volume. The width of the layer is mostly determined by the surface modification of the particle, rather than its size.

The three-phase model predicts small values of the thickness l for the interfacial layer (1.6–2.5 nm). For polymers with nanosized clay this layer was estimated with the electron spin resonance technique to be between 5 and 15 nm [65]. Chen *et al* [66] deduced that the thickness of the interfacial was 5–10 nm for poly(vinyl alcohol)/silica and dependent upon composition. The other estimations [67] for the interfacial thermal conductance between a single crystal silicon and amorphous polyethylene have shown that the interfacial layer of the polymer has a thickness of 16 nm. Calculating the three-phase model with the same interface thickness ($l = 16$ nm) for our experimental systems, we can derive the effective thermal conductivity of the particle + interfacial layer, i.e. CP is smaller as the size of the CP decreases. As shown in table 4, the thermal conductivity λ_F' becomes smaller if the size of the CP decreases, e.g. 0.36 for 22 nm MgO particles opposed to 1.11 for 60 nm AlN particles.

The two-phase model does not take into consideration the surface modification of nanoparticles and its influence on the heat conduction mechanism in NCs. The three-phase model on the other hand does take this into account. The low values of the thermal conductivity, which are shown in table 4, are realistic because of large scattering on the surface of nanoparticles.

Table 2. The fitting parameters of the 2-phase LN models.

Composite	λ_m (W m^{-1} K^{-1})	ξ	λ_f (W m^{-1} K^{-1})	$(1-\phi_M)/\phi_M^2$
ER-Al_2O_3 micro	0.168	10 (7.36)	5 (2.45)	1.34
ER-SiO_2 micro	0.168	4.9	2	1.16
ER-SiO_2 nano	0.168	1.5	1.36	0.89

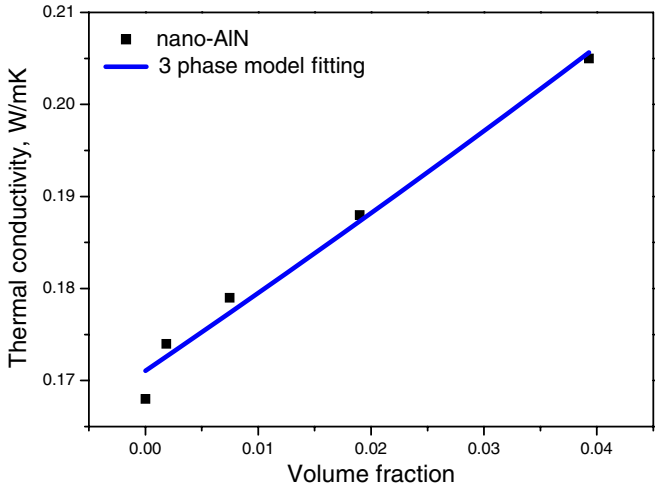

Figure 13. Thermal conductivity of ER-AlN composite as a function of the filler loading (squares) fitted with the 3 -phase LN model (solid line).

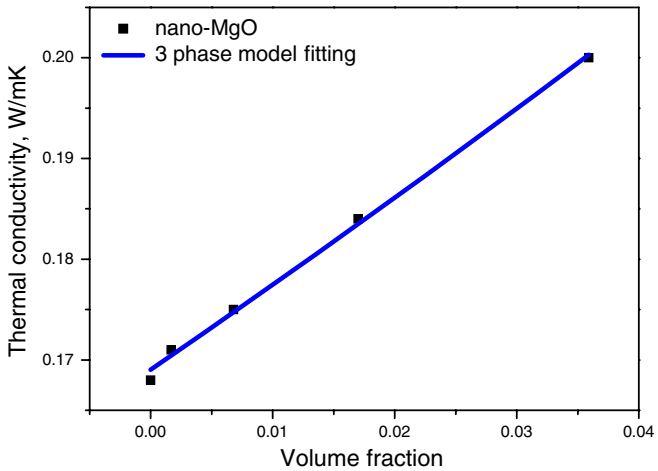

Figure 14. Thermal conductivity of ER-MgO composite as a function of the filler loading (squares) fitted with the 3- phase LN model (solid line).

The three-phase model can be used to predict the thermal conductivity of a composite, which contains surface modified nanoparticles.

The Kapitza thermal resistance, R_K, caused by different phonon scattering processes, is effectively present in the measured value for the thermal conductivity of the CP. In a multiphase system there can be a strong scattering of phonons, which occurs when the phonons propagate through a boundary separating one phase from another. The large interfacial area plays a dominant role for the phonon scattering mechanisms inside a polymer composite. This effect is vanishing with an increasing filler size. However, the effective value for the thermal coefficient of the CP (λ'_F) and the size of CP gives an estimation for R_K. The structure of the equation for the effective thermal conductivity of the CP assumes that we deal with a three-phase model, where the interfacial layer has thermal conductivity λ_l, and a layer thickness l. Although the thermal conductivity of nanoparticles is unknown, the thermal resistance of the layer is $R_K = l/\lambda_l$, effectively introducing the thickness l and the thermal conductivity of the layer. Therefore,

$$\lambda'_F = \lambda_f \Big/ \left(1 + \frac{l\lambda_f}{d\lambda_l}\right). \tag{10}$$

With a fixed value for l, the three-phase model effectively becomes a two-phase model, by giving the interfacial layer the same thermal conductivity as the matrix has, $\lambda_l \to \lambda_m$. In this case we are not getting to $\lambda'_F = \lambda_f$, but a different value dependent on the size of the interfacial layer. Therefore, the only way to achieve this limit is to set $l = 0$. Otherwise, a finite value of $l\lambda_f/\lambda_l d$ may require a renormalization of the volume fraction of the nanoparticles by introducing a new parameter, which is responsible for the interfacial layer.

5. Conclusions

The thermal conductivity of microcomposites is the result of the formation of filler networks at high filler concentrations. The thermal conductivity of the polymer systems containing a small amount of surface modified nanoparticles is controlled by the interfacial polymer layer, which acts as the main heat conduction matter. The size of the interfacial layer depends on the nature of the particle surface. Two- and three-phase Lewis–Nielsen models were used to fit the experimental data. Both models fit the experimental data accurately, but the obtained fitting parameters have not yet been confirmed experimentally. This is due to difficulties in determining the thermal conductivity of the particles, the thickness of the interface layer and its thermal conductivity. The two-phase model is used for fitting the thermal conductivity of systems containing microparticles and nonmodified nanoparticles, while the three-phase model is valuable for a polymer matrix that has been reinforced by surface modified nanofiller. In particular when nanosized fillers are used, the relative surface area of the interface, and thus the volume of the interfacial zone, is significant. Hence, the interfacial zone will determine the thermal conductivity of the system, since it can conduct heat much better than the constituents themselves. That means that ultimately the thermal conductivity is affected more by the interfacial zone than by the polymer and nanoparticles. Currently, the values of some of the unknown parameters of the three-phase model are sought after through different analytical measurements. The precise nature and thickness

Table 3. The fitting parameters of the 3-phase LN model.

Composite	λ_m (W m^{-1} K^{-1})	ξ	λ'_F (W m^{-1} K^{-1})	$(1-\phi_M)/\phi_M^2$	$(\nu_l+\nu_f)/\nu_f$	l (nm)
ER-Al_2O_3 nano	0.171	3.0	2	1.1	1.17	1.6
ER-AlN nano	0.171	3.6	22	1.1	1.10	1.9
ER-MgO nano	0.169	4.3	2	1.0	1.38	2.5

Table 4. The fitting parameters of the 3-phase LN model assuming a 16 nm interfacial layer thickness.

Composite	λ_m (W m^{-1} K^{-1})	ξ	λ'_F (W m^{-1} K^{-1})	$(1-\phi_M)/\phi_M^2$	$(\nu_l+\nu_f)/\nu_f$	l (nm)
ER-Al_2O_3 nano	0.171	2.5	0.38	1.1	3.62	16
ER-AlN nano	0.171	3.1	1.11	1.1	2.03	16
ER-MgO nano	0.169	4.3	0.36	1.1	5.15	16

of the interfacial layer between particle and polymer are not known. Literature shows that the thickness of the layer can be calculated or obtained by indirect measurements. The thickness of the interfacial layer has been used to calculate thermal conductivity of a composite particle, the relative volume of the affected polymer and the shape factor in the three-phase model. In future work we will try to quantify the thickness of this layer and the exact values for the thermal conductivity to make the model more precise.

Acknowledgments

This work is part of the Research Programme of the Dutch Polymer Institute (DPI), Eindhoven, the Netherlands, project #623. The financial support from Dutch government for IOP-EMVT grant is gratefully acknowledged. The authors would like to thank Ben Norder and Ugo Lafont from DelftChemTech for their help in performing measurements.

References

[1] Mark J E 2007 *Physical Properties of Polymers* (Berlin: Springer)
[2] Xie S-H, Zhu B-K, Li J-B, Wei X-Z and Xu Z-K 2004 *Polym. Test.* **23** 797–804
[3] Xu Y and Chung D D L 2000 *Compos. Interface* **7** 243–56
[4] Wong C P and Bollampally R S 1999 *IEEE Trans. Adv. Packag.* **22** 54–9
[5] Bujard P and Ansermet J P 1989 *5th IEEE SEMI-TERM™ Symp. (San Diego, CA)* pp 126–30
[6] Ng H Y, Lu X and Lau S K 2005 *Polym. Compos.* **26** 778–90
[7] Lee E-S, Lee S-M, Shanefield D J and Cannon W R 2008 *J. Am. Ceram. Soc.* **91** 1169–74
[8] Konzelmann S, Hoffmann C, Metre R and Peier D 2008 *IEEE Trans. Dielectr. Electr. Insul.* **15** 327–33
[9] Wong C P and Bollampally R S 1999 *Int. Symp. on Advanced Packaging Materials (Braselton, GA)* pp 113–7
[10] Han Z, Wood J W, Herman H, Zhang C and Stevens G C 2008 *Int. Symp. on Electrical Insulation (Vancouver)* pp 497–501
[11] Yung K C and Liem H 2007 *J. Appl. Polym. Sci.* **106** 3587–91
[12] Zhou W, Qi S, An Q, Zhao H and Liu N 2007 *Mater. Res. Bull.* **42** 1863–73
[13] Kim J K, Kim J W, Kim M I and Song M S 2006 *Macromol. Res.* **14** 517–23
[14] Dong H, Fan L and Wong C P 2005 *Electronic Components and Technology Conf. (Lake Buena Vista, FL)* pp 1451–4
[15] Stevens G C, Herman H, Han J, Wood J W, Mitchell A and Thomas J 2009 *11th Insucon Conf. (Birmingham, UK)* pp 286–91
[16] Garrett K W and Rosenberg H M 1974 *J. Phys. D: Appl. Phys.* **7** 1247–58
[17] He H, Fu R, Han Y, Shen Y and Wang D 2007 *J. Electron. Packag.* **129** 469–72
[18] Agarwal S, Khan M M K and Gupta R K 2008 *Polym. Eng. Sci.* **48** 2474–81
[19] Moniruzzaman M and Winey K I 2006 *Macromolecules* **39** 5194–205
[20] Fukushima K, Takahashi H, Takezawa Y, Hattori M, Itoh M and Yonekura M 2004 *Conf. on Electrical Insulation and Dielectric Phenomena (Boulder, CO)* pp 340–3
[21] Miyazaki Y, Nishiyama T, Takahashi H, Katagiri J-I and Takezawa Y 2009 *Conf. on Electrical Insulation and Dielectric Phenomena (Virginia Beach, VA)* pp 638–41
[22] Ekstrand L, Kristiansen H and Liu J 2005 *28th Int. Spring Seminar on Electronics Technology (Wiener Neustadt, Austria)* pp 19–23
[23] Tavman I H 2000 *Int. Comm. Heat Mass Transfer* **27** 253–61
[24] Irwin P C, Cao Y, Bansal A and Schadler L S 2003 *Conf. on Electrical Insulation and Dielectric Phenomena (Albuquerque, NM)* pp 120–3
[25] Xu J and Wong C P 2005 *Electronic Components and Technology Conf. (Lake Buena Vista, FL)* pp 1234–40
[26] Olhero S M, Novak S, Oliveira M, Krnel K, Kosmac T and Ferreira J M F 2004 *J. Mater. Res.* **19** 746–51
[27] Nielsen L E 1970 *J. Appl. Phys.* **41** 4626–7
[28] Nielsen L E 1973 *J. Appl. Polym. Sci.* **17** 3819–20
[29] Bruggeman D A G 1935 *Ann. Phys., Lpz* **24** 636–79
[30] Maxwell J C 1954 A *Treatise on Electricity And Magnetism* (New York: Dover)
[31] Fricke H 1924 *Phys. Rev.* **24** 575–87
[32] Kochetov R, Andritsch T, Lafont U, Morshuis P H F, Picken S J and Smit J J 2009 *Electrical Insulation Conf. (Montreal)* pp 524–8
[33] Lewis T B and Nielsen L E 1970 *J. Appl. Polym. Sci.* **14** 1449–71
[34] Yang Y, Grulke E A, Zhang Z G and Wu G 2006 *J. Appl. Phys.* **99** 114307
[35] Cherkasova A S and Shan J W 2008 *J. Heat Transfer* **130** 082406-1
[36] Guthy C, Du F, Brand S, Wilney K I and Fischer J E 2007 *J. Heat Transfer* **129** 1096–9
[37] Picken S J, Korobko A V, Mendes E, Norder B, Makarova V V, Vasilyev G B, Karbushev V V and Tolstykh M Yu 2011 *J. Polym. Eng.* **31** 269–73
[38] Prasher R, Evans W, Meakin P, Fish J, Phelan P and Keblinski P 2006 *Appl. Phys. Lett.* **89** 143119
[39] Agari Y and Uno T 1986 *J. Appl. Polym. Sci.* **32** 5705–12
[40] Kumlutas D and Tavman I H 2006 *J. Thermoplast. Compos. Mater.* **19** 441–55
[41] Evans W, Prasher R, Fish J, Meakin P, Phelan P and Keblinski P 2008 *Int. J. Heat Mass Transfer* **51** 1431–8

[42] Andritsch T 2010 Epoxy based nanocomposites for high voltage DC applications. Synthesis, dielectric properties and space charge dynamics *PhD Thesis* TU Delft
[43] Kotsilkova R 2007 *Thermoset Nanocomposites for Engineering Applications* (Slawbury, Shrewsbury, UK: Smithers Rapta technology)
[44] Wang X-Q and Mujumdar A S 2007 *Int. J. Therm. Sci.* **46** 1–19
[45] Chandrasekar M and Suresh S 2009 *Heat Transfer Eng.* **30** 1136–50
[46] Keblinski P, Phillpot S R, Choi S U S and Eastman J A 2002 *Int. J. Heat and Mass Transfer* **45** 855–63
[47] Yu W and Choi S U S 2003 *J. Nanopart. Res.* **5** 167–71
[48] Xue Q and Xu W-M 2005 *Mater. Chem. Phys.* **90** 298–301
[49] Nan C-W, Birringer R, Clarke D R and Gleiter H 1997 *J. Appl. Phys.* **81** 6692–9
[50] Bowen P, Highfield J G, Mocellin A and Ring T A 1990 *J. Am. Ceram. Soc.* **73** 724–8
[51] Waldman B A 1996 *Mod. Paint Coating.* **86** 34–8
[52] Petrie E M 2006 *Handbook of Adhesives and Sealants* (New York: McGraw-Hill)
[53] Akil H M, Lily N, Razak J A, Ong H and Ahmad Z A 2006 *J. Reinf. Plast. Compos.* **25** 745–59
[54] Shokoohi S, Arezafar A and Khosrokhavar R 2008 *J. Reinf. Plast. Compos.* **27** 473–85
[55] Lee E-S, Lee S-M, Cannon R and Shanefield D J 2008 *Colloid. Surf.* A **316** 95–103
[56] Maity P, Kasisomayajula S V, Parameswaran V, Basu S and Gupta N 2008 *IEEE Trans. Dielectr. Electr. Insul.* **15** 63–72
[57] Mai Y-W and Yu Z-Z 2006 *Polymer Nanocomposites* (Cambridge: Woodhead Publishing Limited)
[58] Friedrich K and Schlarb A K 2008 *Tribology of Polymeric Nanocomposites: Friction and Wear of Bulk Materials and Coatings* (Amsterdam: Elsevier)
[59] Shindé S L and Goela J S 2006 *High Thermal Conductivity Materials* (Berlin: Springer)
[60] Lee H and Neville K 1957 *Epoxy Resins: their Applications and Technology* (New York: McGraw-Hill)
[61] Andritsch T, Kochetov R, Morshuis P H F and Smit J J 2010 *Conf. on Electrical Insulation and Dielectric Phenomenon* pp 530–3
[62] Kochetov R, Andritsch T, Morshuis P H F and Smit J J *IEEE Trans. Dielectr. Insulation Mater.* submitted
[63] Tavman I H 1998 *Int. Commun. Heat Mass Transfer* **25** 723–32
[64] Van Es M A 2001 Polymer-clay nanocomposites, the importance of particle dimensions *PhD Thesis* TU Delft
[65] Miwa Y, Drews A R and Schlink S 2006 *Macromolecules* **39** 3304–10
[66] Chen L, Zheng K, Tian X, Hu K, Wang R, Liu C, Li Y and Cui P 2010 *Macromolecules* **43** 1076–82
[67] Hu M, Shenogin S and Keblinski P 2007 *Appl. Phys. Lett.* **91** 241910